BASIC SCIENCE

Nanomedicine: Nanotechnology, Biology, and Medicine
19 (2019) 95–105

Original Article

nanomedjournal.com

Delivery of biologically active miR-34a in normal and cancer mammary epithelial cells by synthetic nanoparticles

Fabiana Panebianco, BSc[a], Montserrat Climent, PhD[a], Mari Ada Malvindi, PhD[b], Pier Paolo Pompa, PhD[b,c], Paola Bonetti, PhD[a,*,1], Francesco Nicassio, PhD[a,*,1]

[a]*Center for Genomic Science of IIT@SEMM, Istituto Italiano di Tecnologia (IIT), Milan, Italy*
[b]*Nanobiointeractions & Nanodiagnostics, Center for Biomolecular Nanotechnologies@UniLe, Istituto Italiano di Tecnologia, Arnesano (Lecce), Italy*
[c]*Nanobiointeractions & Nanodiagnostics, Istituto Italiano di Tecnologia, Genoa 16163, Italy*

Abstract

Functional RNAs, such as microRNAs, are emerging as innovative tools in the treatment of aggressive and incurable cancers. In this study, we explore the potential of silica dioxide nanoparticles (SiO_2NPs) in the delivery of biologically active miRNAs. Focusing on the tumor-suppressor miR-34a, we evaluated miRNAs delivery by SiO_2NPs into the mammary gland, using *in vitro* as well as *in vivo* model systems. We showed that silica nanoparticles can efficiently deliver miR-34a into normal and cancer epithelial cells grown in culture without major signs of toxicity. Delivered miRNA retained the ability to silence artificial as well endogenous targets and can reduce the growth of mammospheres in 3D culture. Finally, miR-34a delivery through intra-tumor administration of SiO_2NPs leads to a reduced mammary tumor growth. In conclusion, our studies suggest that silica nanoparticles can mediate the delivery of miR-34a directly into mammary tumors while preserving its molecular and biological activity.

Key words: miRNA; RNA delivery; Nanoparticles; Mammary gland; Stem cells; Breast cancer

MicroRNAs (miRNAs) are small (18–22 nucleotides long) regulatory non-coding RNAs that function post-transcriptionally in gene expression regulation.[1] Typically, silencing occurs in the cytosol and requires the miRNA to be loaded on to the RNA induced silencing complex (RISC) and interacting by complementarity with a matching region on the target RNA, known as the miRNA responsive element (MRE) and located in the 3′ untranslated region.[2] miRNAs have emerged as critical hubs in gene expression regulation, able to influence most, if not all, cellular processes, including cell proliferation, differentiation and apoptosis. Furthermore, by acting as either oncogenes ('oncomiRs') or tumor suppressors, miRNAs have been frequently and closely associated with the pathogenesis of cancer.[3] Since they are able to simultaneously extinguish the expression of a multitude of genes, miRNAs are considered to be promising therapeutics with cancer-specific effects.[3,4] Relevant examples include: the let-7 family of miRNAs, frequently down-regulated in a variety of cancers, and shown to inhibit cancer progression when ectopically administered[5]; the oncogenic miR-21, up-regulated in human cancer and shown to induce pre-B cell lymphoma, providing evidence for oncomiR addiction[6]; the tumor-suppressor miR-34 family, a downstream component of the p53 network,[7] inhibited in various solid malignancies .[8,9] In the case of breast cancers, miR-34a, a component of the miR-34 family, has been shown to inhibit both

This work was supported by grants from the Associazione Italiana per la Ricerca sul Cancro (AIRC—G14085 and IG18774 to FN) and Cariplo (2015-0590) to F.N.

Acknowledgements: We thank the Imaging Unit for performing FACS experiments, Matteo J Marzi, Chiara Tordonato and other lab members for helpful discussion and Claudia Crovace for editing the manuscript.

*Corresponding authors at: Center for Genomic Science of IIT@SEMM, Istituto Italiano di Tecnologia (IIT), c/o Campus IFOM-IEO, Via Adamello 16, 20139, Milan, Italy.

E-mail addresses: paola.bonetti@iit.it, (P. Bonetti), francesco.nicassio@iit.it. (F. Nicassio).

[1] Contributed equally.

https://doi.org/10.1016/j.nano.2019.03.013

Please cite this article as: Panebianco F, et al, Delivery of biologically active miR-34a in normal and cancer mammary epithelial cells by synthetic nanoparticles. *Nanomedicine: NBM* 2019;19:95-105, https://doi.org/10.1016/j.nano.2019.03.013

tumor growth, invasion, metastasis and stemness properties[10–14] thus attracting attention as a therapeutic target. Recently, our own work on the physiological role of miR-34a in mouse and human breast models has added another fragment to the overall picture. Indeed, we have revealed that miR-34a plays a dual role in the mammary gland by controlling both cell proliferation and commitment to differentiation.[15] Consequently, miR-34a administration could inhibit the growth of tumoral cells and the expansion of the stem cell pool,[15] the latter being of crucial importance in tumor relapse and metastasis.[16]

The major challenge posed by miRNA-based therapies is, however, the successful *in vivo* delivery of biologically active molecules. Delivery methods routinely used in research, like transfection or lentiviral infection, are unsuitable to actual clinical settings, where instead one of the following strategies are currently employed: direct administration of miRNA molecules that have been chemically modified to make them stable *in vivo* and reduce their susceptibility to degradation by RNAses[17]; use of non-pathogenic viral vectors (*e.g.* Adeno Associated Vectors – AAV), encoding the small RNA of interest; or development of synthetic carriers (*i.e.* nanoparticles) that encapsulate RNAs for protection and allow their delivery into cells by internalization.[18,19] Nanoparticles developed for clinical applications are typically made out of synthetic materials and between 5 and 200 nm in diameter, a critical parameter in biodistribution and cellular uptake.[20,21] They can be divided into three main categories: inorganic nanoparticles (*i.e.* gold, silica, carbon, iron oxide), organic nanoparticles (*i.e.* liposomes, chitosan, peptide nanomaterials) and polymer based nanomaterials (*i.e.* PEI, dendrimers, PLGA).[22] Synthetic materials present considerable advantages as vehicles for miRNA delivery due to their simplified manufacturing and to the possibility to control their composition and to make improvements by simply modifying particle size and surface properties.[23] In particular, silica dioxide nanoparticles (SiO_2NPs), which consist of amorphous silica aggregates, possess great versatility, high biocompatibility and low cytotoxicity,[24–28] and are able to function as carrier for the delivery of DNA or siRNA both *in vitro* [[29–31] and *in vivo* models.[27] Based on the evidence and considerations above, we decided to employ SiO_2NPs as carrier in the delivery of miR-34a to breast cells. In view of potential clinical applications, we analyzed both the amount and the biological activity of the miRNA molecules delivered by SiO_2NPs to relevant cellular models, such as cell lines and primary cultures, and to complex environments with resemblance to the real physiology and pathology of the breast, such as 3D models or *in vivo* tumors.

Methods

Synthesis and preparation of SiO2NPs

Fluorescent SiO_2NPs were produced in Dr. Pompa's lab, as described[25] and Supplemental Material. The sequences of the oligos used are: Scramble 5′-CGCUGAGUACUUCGAAAUGUC-3′ and miR-34a 5′-UGGCAGUGUCUUAGCUGGUUGU-3′. In order to avoid formation of aggregates, SiO_2NPs were sonicated for 5 cycles (30 sec on, 30 sec off) in a water-bath sonicator (Bioruptor ucd 300 plus - DIAGENODE), diluted and sonicated again. In the case of treatments in culture, SiO_2NPs were added to cells for 5 hours in absence of serum to favor their internalization. After incubation, cells were washed and kept in culture with normal medium at 37 °C. In the case of *in vivo* treatments, SiO_2NPs were resuspended in PBS.

Cell cultures and reagents

Primary mouse mammary epithelial cells (MMECs) were dissected from 8 to 10 weeks old virgin females as previously described[32] and Supplemental Material. Comma Dβ cells were cultured in 1:1 DMEM/F12 (Gibco BRL) with 2% FBS, 2 mM L-glutamine (Gibco BRL), 10 μg/ml bovine insulin (Sigma) and 5 ng/ml EGF (Sigma).[33] SUM159pt (Asterand, Detroit, MI) were cultured in Ham's F12 medium with 5% FBS, 2 mM L-glutamine, 5 μg/ml insulin, 1 μg/ml hydrocortisone and 10 mM HEPES and incubated at 37 °C with 10% CO2 in incubator. For the proliferation curve, 10^5 Comma Dβ and SUM159pt were plated in triplicates and counted on day 1, 4 and 7 after treatments. When transfecting oligo RNAs, the Hyperfect (Qiagen) was used. The lentiviral miR-34a sensor was a gift from Naldini's laboratory.[34] To produce the lentivirus, HEK293T were transfected in 15 cm plates with 10 μg of pRSV-Rev, 10 μg of pMDLg/pRRE (gag&pol), 10 μg of pMD2.G (VSV-G), 20 μg of the vector, and 250 μl of 2 M $CaCl_2$ in a final volume of 2 ml TE 0.1×. To increase virus titer, supernatant was collected 36 h post-transfection, filtered at 0.45 μm and ultracentrifuged for 2.5 h at 20000 rpm at 4 °C, then the pellet was resuspended in PBS. The viral stock was frozen (−80 °C) or used fresh to infect 200,000 target cells at a ratio of 30 μl virus in the presence of 1 μg/mL polybrene.

Flow cytometry

Cells were harvested after SiO_2NPs treatment and fixed in 1% formaldehyde (Sigma) for 15 min on ice, washed and resuspended in PBS. For miR-sensor analysis, cells were harvested and stained against ΔNGFR (CD271-PeCy7; BD Pharmingen). When analyzing cell death, cells were collected, washed and incubated with AnnexinV-APC (eBiosciences) for 45 min and immediately analyzed. DAPI was (Sigma) added just before acquisition. FACS analysis was performed using MACSQuant Flow cytometer (Mylteni) and data analysis by FlowJo (TreeStar).

In vivo studies

The miR-34TKO mouse strain was generated in Ventura's laboratory,[35] and the Trp53 strain was purchased from Jackson laboratories (stock #002101); both are in the C57/BL6J background. Immunodeficient NOD.Cg-*Prkdc*^{scid}*Il2rg*^{tm1Wjl}/SzJ mice (NSG, Charles River) were used for transplantation. SUM159pt were resuspended with 50,000 cells in 20 μL of 1:3 Matrigel® (BD Biosciences): PBS. 6–8 weeks-old NSG females were anesthetized with 2.5% Avertin in PBS (stock solution Avertin: 10 g of tribromoethanol (Sigma) in 10 ml of tertamyl alcohol (Sigma-Aldrich) by intraperitoneal injection (i.p.) and cells were injected intra-nipple. NPs treatment started when tumors were 8 mm in diameter. Before treatments, NPs were resuspended in PBS at a concentration of 20 mg/kg and sonicated again before use. NPs were injected intra-tumor for 3 consecutive days, 2 weeks in a row. Tumor growth was periodically monitored through caliper measurements. Animals were euthanized at the endpoint and tumors collected. All animal studies were conducted with the approval of Italian Minister

of Health (12/2012 and 762/2015-PR) and were performed in accordance with the Italian law (D.lgs.26/2014), which enforces Dir. 2010/63/EU (Directive 2010/63/EU of the European Parliament and of the Council of 22 September 2010 on the protection of animals used for scientific purposes).

Microscopy

Comma Dβ cells and mammospheres were plated on coverslips pre-treated with polylysine. After incubation with SiO_2NPs, coverslips were washed and fixed with 4% PFA for 15 min at RT, permeabilized with Triton-X100 (BDH Prolabo) for 5 min and incubated with DAPI for 5 min. Finally, coverslips were mounted with Mowiol. To detect NPs in the whole mammary gland, mice were sacrificed 24 h after treatment and mammary glands collected and placed onto glass covers (ThermoScientific), fixed with 4% PFA for 24 h at 4 °C, washed and stained with DAPI for 1 h. For fluorescent microscopy, images were taken using an Upright Olympus AX70. For confocal microscopy, a Leica TCS-SP2 was used.

Statistics

Microsoft Excel was used to generate bar graphs with average and standard deviation (SD) of repeated experiments and to calculate statistical significance (Student's or Welch's T-test). The number of replicates and the statistical tests used are indicated in figure legends.

Results

Mammary epithelial cells efficiently internalize silica nanoparticles both in 2D and 3D growth

At first, we tested internalization and toxicity effects of SiO_2 nanoparticles (SiO_2NPs) on mammary epithelial cells. We used two different models: i) a normal mammary epithelial cell line (Comma Dβ, murine), and ii) a cancer cell line from a claudine-low triple-negative breast cancer (SUM159pt, human). To evaluate internalization, we exploited the fluorescence emitted by SiO_2NPs doped with a fluorophore (Figure 1, *A*).[25] We observed a typical cytoplasmatic/perinuclear distribution of SiO_2NPs just 24 hours after treatment[29] (Figure 1, *B*). FACS analysis revealed that SiO_2NPs had been efficiently internalized by most cells, with a higher dose of SiO_2NPs producing higher internalization (Figure 1, *C* and *D*). The percentage of cells exhibiting fluorescence decreased over time (4 and 7 days), probably due to a significant dilution of SiO_2NPs by cell division and/or exocytosis[36] (Figure 1, *E*). Similarly to a previous work done on different epithelial cell types,[29] in our study mammary epithelial cells did not show signs of toxicity upon treatment with SiO_2NPs. Indeed, the growth rate did not change when comparing untreated cells with cells treated for up to 6 days with 0.25 or 1 nM SiO_2NPs (Figure 1, *F*). This observation was further confirmed when measuring cell viability through Annexin V staining, as neither the percentage of apoptotic cells nor the percentage of necrotic cells increased upon treatment (Figure 1, *G*). We next tested nanoparticle internalization in a physiologically relevant model, namely primary epithelial cells isolated from the mammary gland of wild-type mice and grown in 3D liquid culture as mammospheres, a condition selective for mammary stem cells (Figure 2, *A*,[37]). SiO_2NPs were efficiently internalized by mammospheres when observed by FACS analysis (Figure 2, *B* and *C*). The effect was dose-dependent, similarly to what observed in cells grown in 2D and the fluorescence signal persisted for up to 7 days (Figure 2, *D*), as cells are slowly dividing. In addition, fluorescence was visible both in the spheroids' inner part, which contains stem-cells and early progenitors, and in their outer part, which contains more differentiated cells (Figure 2, *E*; Figure S1B). SiO_2NPs treatment did not induce toxicity in mammospheres as they appeared similar in size and shape to those from untreated cells (not shown). Indeed, sphere formation efficiency (SFE), which reflects the capability of mammary stem cells to re-form spheroids once re-plated as a single-cell suspension, was not altered (Figure 2, *F*). Overall, these results indicated that SiO_2NPs are biocompatible with mammary epithelial cells and could be efficiently internalized by organoids.

Delivery of miR-34a by SiO_2NPs

We next tested SiO_2NPs for the ability to deliver functional miRNAs into mammary cells. To this aim, we functionalized fluorescent SiO_2NPs with amine groups as previously described,[29] to allow binding of nucleic acids (including miRNAs) by electrostatic interaction (Figure 3, *A*). We analyzed morphology and size dispersion of the nanoparticles by transmission electron microscopy (TEM, Figure 3, *B*), checked the absorption/emission spectrum (Figure 3, *C*) and confirmed the change in the net surface charge by zeta potential measurements (Figure 3, *D*). We then mixed 100 μg of 50 nM SiO_2NPs with increasing amounts of RNA oligonucleotides (0.018–0.148 μmol), using a synthetic mature miRNA-34a sequence or a control scramble (SCR) sequence, in order to generate nanoparticles functionalized with either of the oligonucleotides (34a-NPs and SCR-NPs, respectively). After 2 hours of incubation, RNA/SiO_2NPs mixtures were analyzed by gel electrophoresis (Figure 3, *E*). Free RNA (lane 6) migrated through the gel whereas RNAs mixed with SiO_2NPs (lane 2–5) stayed in the loading well, indicating that the RNA was adsorbed onto the SiO_2NPs surface. This was further confirmed by the difference in surface charge observed between amine modified fluorescent SiO2NPs (net positive charge) and RNA/SiO2NPs (net negative charge) (Figure 3, *D*) Subsequently, we evaluated whether SiO_2NPs were able to efficiently deliver miR-34a into the cells. FACS analysis showed that both 34a-NPs and SCR-NPs had been efficiently and similarly internalized into all cell models (Comma Dβ, Sum159pt and Mammospheres) 24 hours after treatment and when used at 1 nM (Figure 4, *A–C*). Next, we evaluated the specificity of miR-34a delivery by measuring miRNA levels in cells treated with 0.5 and 1 nM of SiO_2NPs, corresponding to 37 and 74 nM of oligonucleotide (miR-34a or SCR) respectively. To calculate the number of miR-34a copies in the cell (absolute quantification), we generated a calibration curve by performing RT-qPCR on a miR-34a synthetic oligonucleotide at different concentrations (Figure 4, *D*). After 24 hours, Comma Dβ cells treated with SiO2NPs showed a significant increase in the number of miR-34a copies in comparison to either not treated (NT) or SCR-NPs-treated cells (Figure 4, *E*). Importantly, the

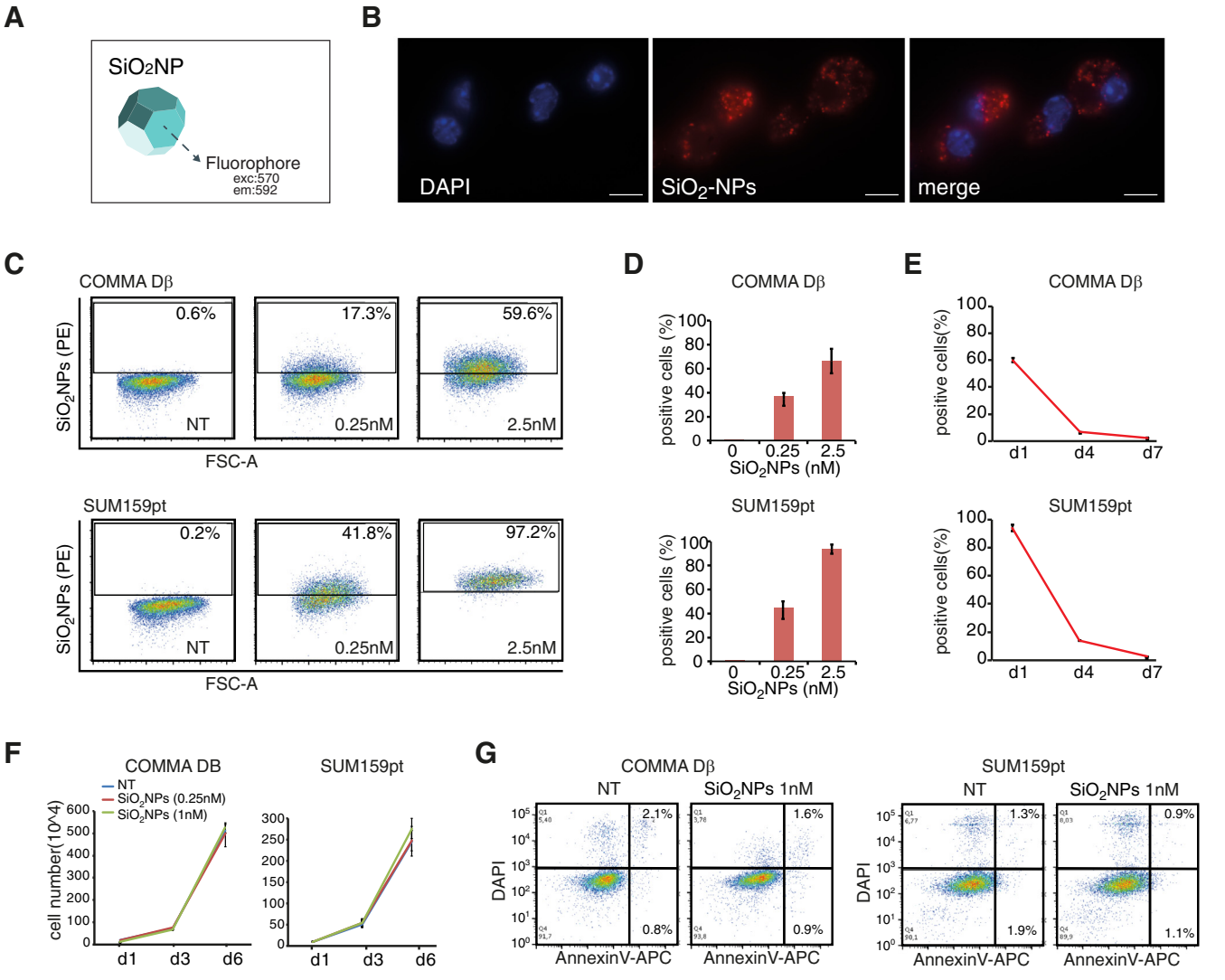

Figure 1. Characterization of SiO_2NPs internalization and toxicity effects on mammary cells. (A) Representative scheme of SiO_2NPs. (B) Pictures of Comma Dβ cells after SiO_2NPs treatment (1 nM, 24 hours). Scale bar 10 μM. (C) Internalization of SiO_2NPs measured by FACS analyses in Comma Dβ and SUM159pt cells at 24 h and using different concentrations of SiO_2NPs (0.25 and 2.5 nM). (D) Percentage of SiO_2NPs positive cells (average and st.dev.) in two independent experiments. (E) SiO_2NPs positive cells (% of total) at 1, 4 and 7 days after treatment with SiO_2NPs (at 2.5 nM). (F) Proliferation of mammary cells at 1, 3 and 6 days after treatment with SiO_2NPs (0.25 and 1 nM). (F) Cell death after prolonged (6 days) treatment with SiO_2NPs (1 nM) measured by FACS. Highlighted the percentage of necrotic ($DAPI^-/AnnexinV^+$) and apoptotic cells ($DAPI^+/AnnexinV^+$).

number of miR-34a copies per cell was proportional to the concentration of NPs (Figure 4, *E*). However, the amount of miRNA delivered into the cells did not match the levels obtained using the same concentrations of miR-34a oligo (37 and 74 nM, Figure 4, *E*) and an optimal transfection system (*i.e.* lipofection with HyperFect, Qiagen). This suggested that the lipofection system is more efficient than the SiO_2NPs when it comes to the total amount of miRNA delivered into the cellular type under study. A similar experiment was performed on primary mammospheres maintained in 3D culture conditions and obtained from mammary glands of either wild-type (WT) or p53 null (p53 –/–) donor mice, the latter known for having very low levels of miR-34a.[35] In both cases the concentration of miR-34a was strongly increased upon 34a-NPs treatment, with no change observed when employing SCR-NPs (Figure 4, *F* and *G*). The effects were almost comparable to those obtained by transfection and the levels of miR-34a remained high even at later time points (96 hours post treatment, Figure 4, *F* and *G*). In conclusion, miR-34a- functionalized SiO_2NPs are able to efficiently deliver miR-34a both into mammary epithelial cells growing in monolayer and into those forming spheroids in a 3D culture.

Biological activity of miR-34a delivered through SiO_2NPs

We next evaluated whether the amount of miRNA delivered by SiO_2NPs was sufficient to trigger the biological activities associated with miR-34a. At first, we measured miRNA activity

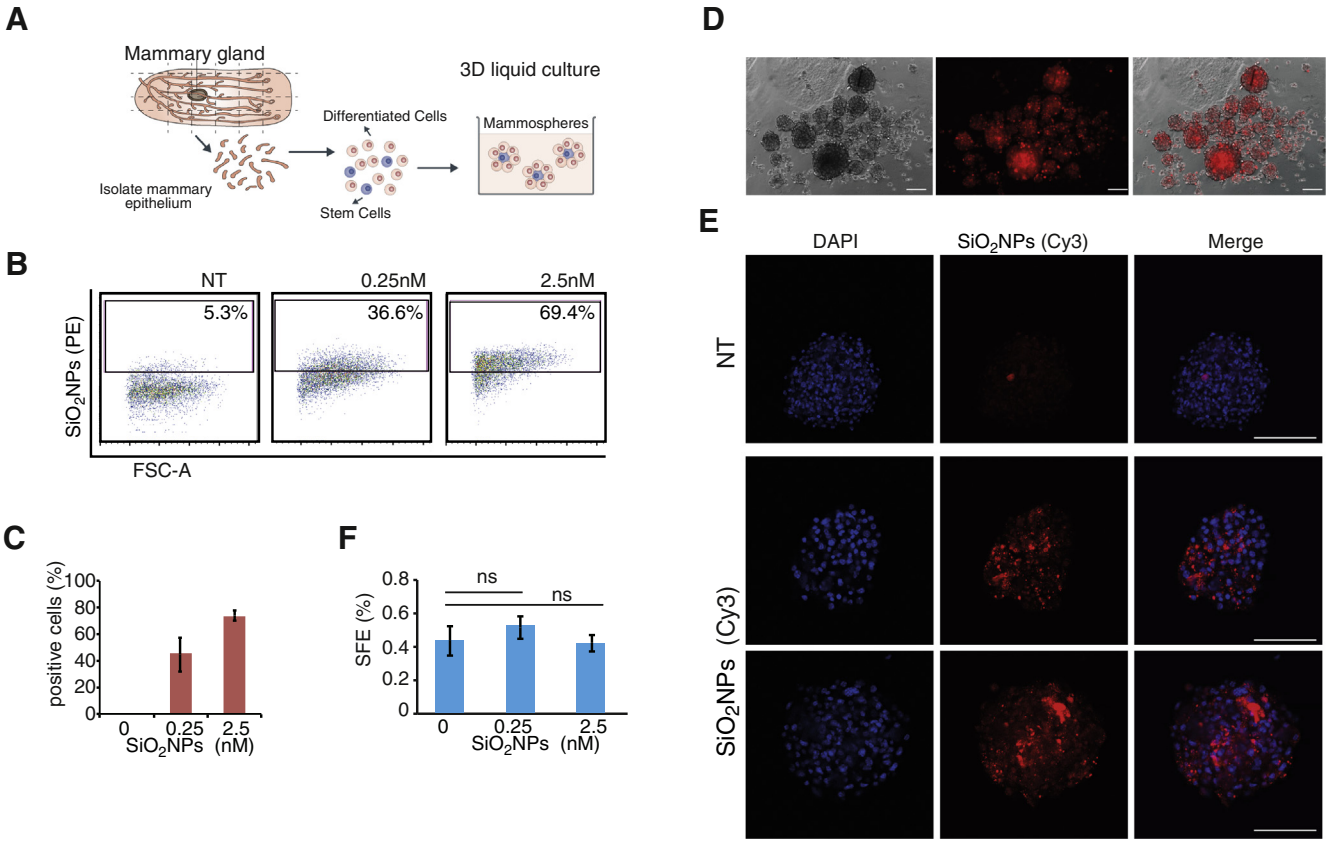

Figure 2. Characterization of SiO_2NPs internalization and toxicity effects on mammospheres. (A) Schematic representation of the strategy for isolation and cultivation of primary mammospheres from mammary gland. (B) Internalization of SiO_2NPs measured by FACS at 24 hours and using two different concentrations of SiO_2NPs (0.25 and 2.5 nM). (C) Percentage of SiO_2NPs positive cells (average and st.dev.) in two independent experiments. Representative images by wide-field (D) or confocal (E) microscopy of mammospheres obtained from primary mammary epithelial cells from wild-type (C57/BL6J) mice and grown for 7 days after SiO_2NPs treatment (1 nM). Red fluorescence shows the accumulation of SiO_2NPs within cells. Scale bar 200 μM. (F) Sphere-forming efficiency (SFE, %) of mammospheres grown with SiO_2NPs.

using a GFP reporter system known as 'miR-sensor' (Figure 5, *A*). It consists of a lentiviral backbone expressing a GFP transgene that is responsive to a specific miRNA (in this case miR-34a) through the presence, in its 3' UTR, of four perfect miRNA binding sites. The miR-sensor also contains a second ΔNGFR transgene (a truncated form of the Nerve Growth Factor Receptor – NGFR) which serves to normalize for transduction efficiency.[34] In our reporter system, the amount of GFP protein produced is controlled by the abundance of miR-34a in the cell: the more abundant is miR-34a, the less expressed is the GFP protein. Therefore, GFP fluorescence measured by FACS is a proxy for miR-34a activity. We infected Comma Dβ cells with either Sensor-34a or a control sensor (Sensor-CTR) and treated them with either 34a-NPs or SCR-NPs (1 nM). Following treatment, we analyzed GFP levels through FACS analysis at 24 hours. As expected, 34a-NPs treatment did not alter GFP signal in cells transduced with Sensor-CTR (Figure 5, *B*), whereas it significantly reduced GFP levels in cells infected with Sensor-34a (Figure 5, *C*). Importantly, this effect was comparable to and almost undistinguishable from that obtained transfecting cells by lipofection (74 nM, Figure 5, *C*) and using either our miR-34a synthetic oligo or a commercially available one (mimic-34a, Qiagen). Hence, although the amount of miR-34a delivered, by SiO_2NPs was lower than that delivered by lipofection (see Figure 4, *E*), the effects produced were similar with respect to specific miRNA activity. Subsequently, we tested the activity of miR-34a by studying the silencing effects on its RNA targets. We considered several of previously validated miR-34a targets[38] and measured their expression at the level of mRNA (RT-qPCR, Figure 5, *D*) or protein (western blot, Figure 5, *E*). The levels of some of these targets were significantly reduced following either transfection or nanoparticle-mediated delivery, without much difference in the extent of regulation (Figure 5, *D* and *E*). In particular, Notch1, a well-established miR-34a target with an important role in regulating stem cell functions and luminal differentiation,[39] resulted the most down-regulated both at mRNA and protein level. Finally, we checked whether miR-34a delivered by SiO_2NPs was able to modulate biological properties in the targeted cells. We used mammospheres as model and focused on their self-propagation ability, which relies on the presence of a stem cells pool. We and others showed that ectopic expression of miR-34a can limit the propagation of normal as

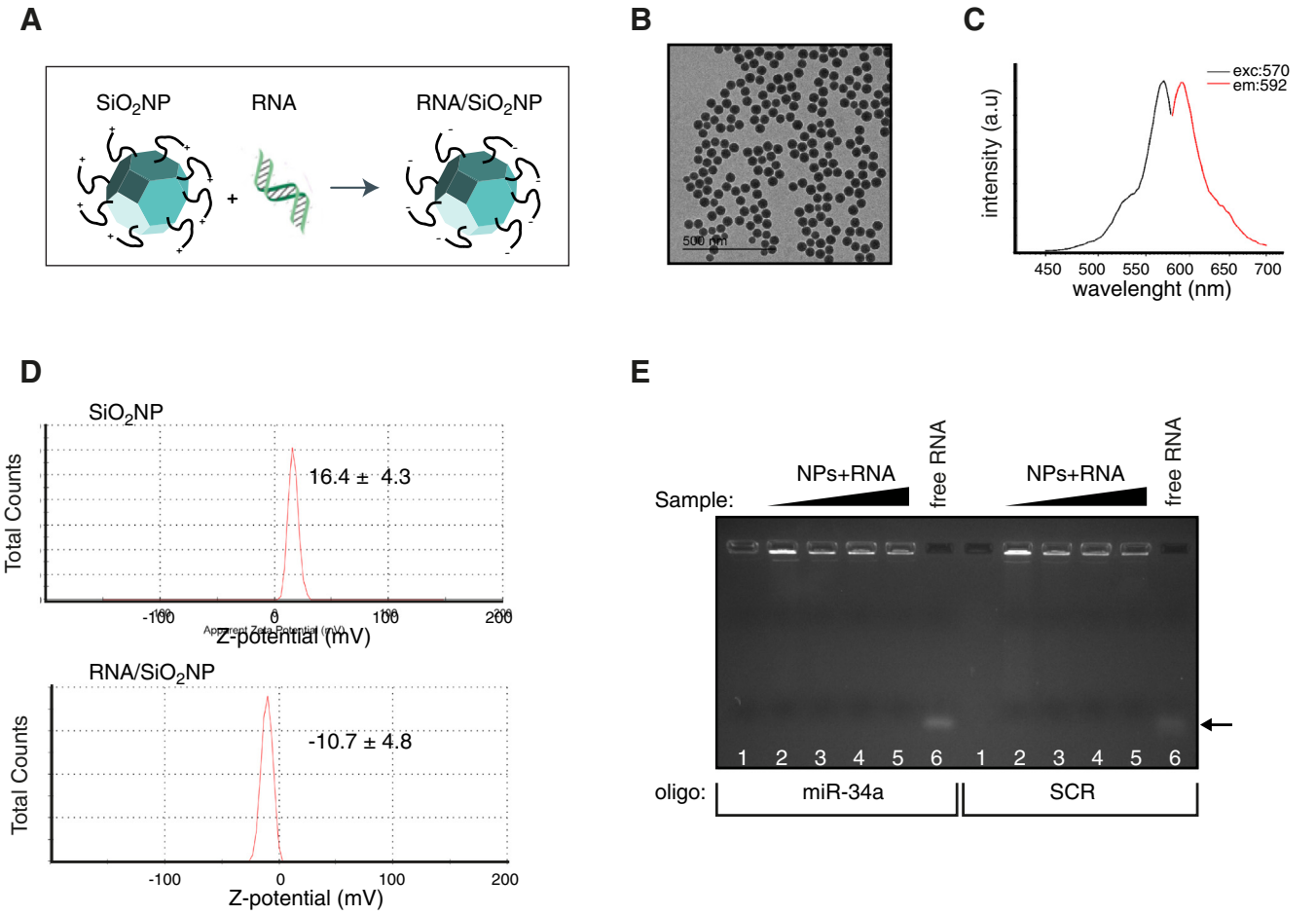

Figure 3. Chemical–physical characterization of Amine modified Fluorescent SiO_2NPs. (A) Representative scheme of strategy for SiO_2NPs functionalization with miRNA mimics. (B) Transmission electron microscopy (TEM) analysis of SiO_2NPs. Uniform morphology and size dispersion was shown. (C) Spectroscopic characterization of SiO_2NPs: absorption at 570 nm wavelength and emission at 592 nm wavelengths. (D) Zeta (Z)-Potential measurements representing the presence of amine groups on the surface of the SiO_2NPs (upper panel) and zeta (Z)-Potential of modified fluorescent SiO_2NPs mixed with 1 μg of dsRNA (lower panel). (E) Agarose gel was used to check for the migration patterns of RNA/SiO_2NPs complexes obtained by mixing increasing amount of miRNA oligo (0.25, 0.5, 1 and 2 μg) with 100 μg of 50 nM amine modified fluorescent SiO_2NPs. Samples have been resolved by gel electrophoresis for 60 min at 100 V. Lane 1: SiO_2NPs alone; Lane 2–5: SiO_2NPs mixed with 2, 1, 0.5, 0.25 μg of RNA, respectively; Lane 6: free RNA.

well as of cancer stem cells ([15,40,41]), an effect that can be measured *in vitro* through the sphere forming assay. We thus treated mammospheres derived from either wild-type (WT) or p53 null mice (p53−/−) with SCR-NPs or 34a-NPs and let them grow as 3D spheroids for a week, taking the number of spheroids as proxy for the number of stem cells. We observed a significant reduction in sphere formation efficiency (SFE) upon treatment with 34a-NPs in WT and p53 null mammospheres (Figure 5, *F* and *G*). In addition, the reduction obtained using NPs was in the same range of that obtained by transfection. We can thus conclude that, even if SiO_2NPs are able to carry a lower amount of microRNA compared to lipofection systems, the biological activity exerted by the miRNA is comparable in both delivery systems, suggesting that not all molecules carried by lipofectamine are loaded on RNA induced silencing complex and consequently are not-functional. Collectively, these data strongly supported the use of SiO_2NPs in the delivery of biologically active miRNAs into mammary epithelial cells.

In vivo miR-34a delivery by SiO_2NPs reduces breast cancer in engrafted mice

We then examined SiO_2NPs as carriers for *in vivo* miRNA delivery. We first evaluated SiO_2NPs uptake in the mammary gland of young (8–10 weeks) mice following intra-nipple injection. We used different amounts of SiO_2NPs and analyzed mammary glands at 24 hours after single treatment, measuring through FACS analysis the percentage of cells that had internalized SiO_2NPs. We observed a significant percentage of positive cells only at the highest concentration of SiO_2NPs (350 μg– corresponding to a dose of 20 mg/kg) (Figure 6, *A*). Fluorescence signal strongly decreased after 4 days, with only a few positive cells detected (Figure 6, *B*), which might suggest clearance of SiO_2NPs, although literature suggests that SiO2-NPs degrade slowly, releasing low amounts of silicic acid, a non-toxic compound naturally found in numerous tissues and efficiently excreted from the body in the urine when

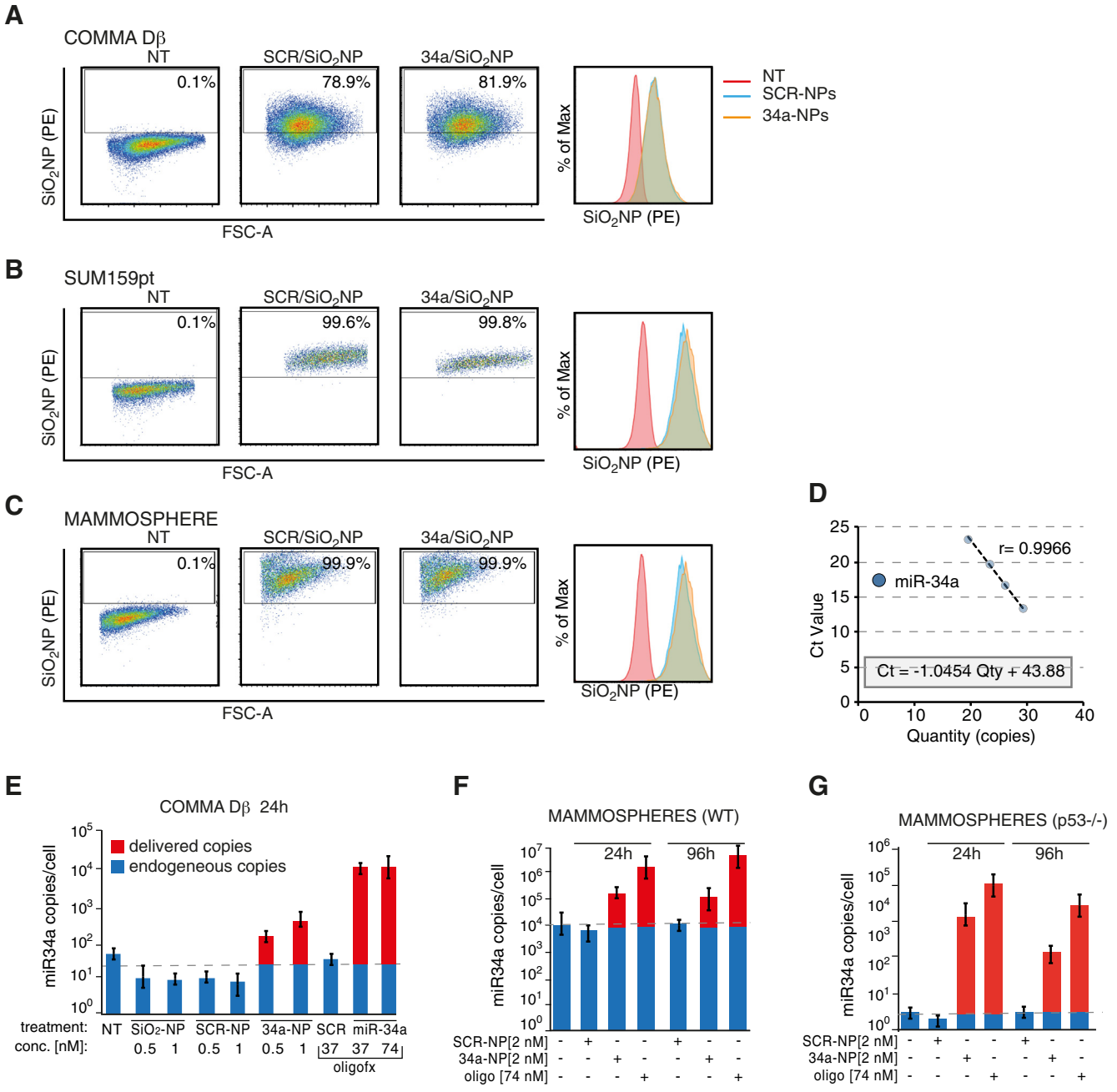

Figure 4. SiO_2NPs cellular uptake *in vitro.* (A-C) FACS analysis showing the internalization of SCR-NPs and 34a-NPs in Comma Dβ (A), SUM159pt (B) and primary mammospheres (C) from wild type mice 24 hours after treatment with 1 nM of SiO_2NPs. Not treated (NT) samples were used as control. (D) Calibration curve for miR-34a absolute quantification by RT-qPCR. Shown the linear fitting, with equation and coefficient of determination (r). (E-G) Quantification of miR-34a delivery by SiO_2NPs in Comma Dβ (panel E), mammospheres from wild-type (WT, panel F) or p53-null mice (p53−/−, panel G) measured as copies per cells and determined by RT-qPCR.

administered to humans.[27,28] Confocal microscopy analysis on the whole tissue confirmed the homogenous distribution of fluorescent cells around the injection site (Figure 6, *C*). We then evaluated the capacity of SiO_2NPs to carry miR-34a *in vivo* by injecting 34a- or SCR-NPs (20 mg/kg) into the mammary glands of mutant miR34-TKO mice[35] that did not express any miR-34a. We observed a significant increase in miR-34a levels in isolated mammary epithelial cells ($Epcam^+/Lin^-$) after 1 day (Figure 6, *D*). Finally, we evaluated the delivery of miR-34a within mammary tumors. For this purpose, we injected SUM159pt cancer cells into the nipple of immunocompromised (NSG) mice, thus generating a palpable solid tumor in few weeks (2–3). SiO_2NPs were injected directly in the tumor and were visible by *in vivo* fluorescence imaging (Figure 6, *E*). Treatment with 34a- or

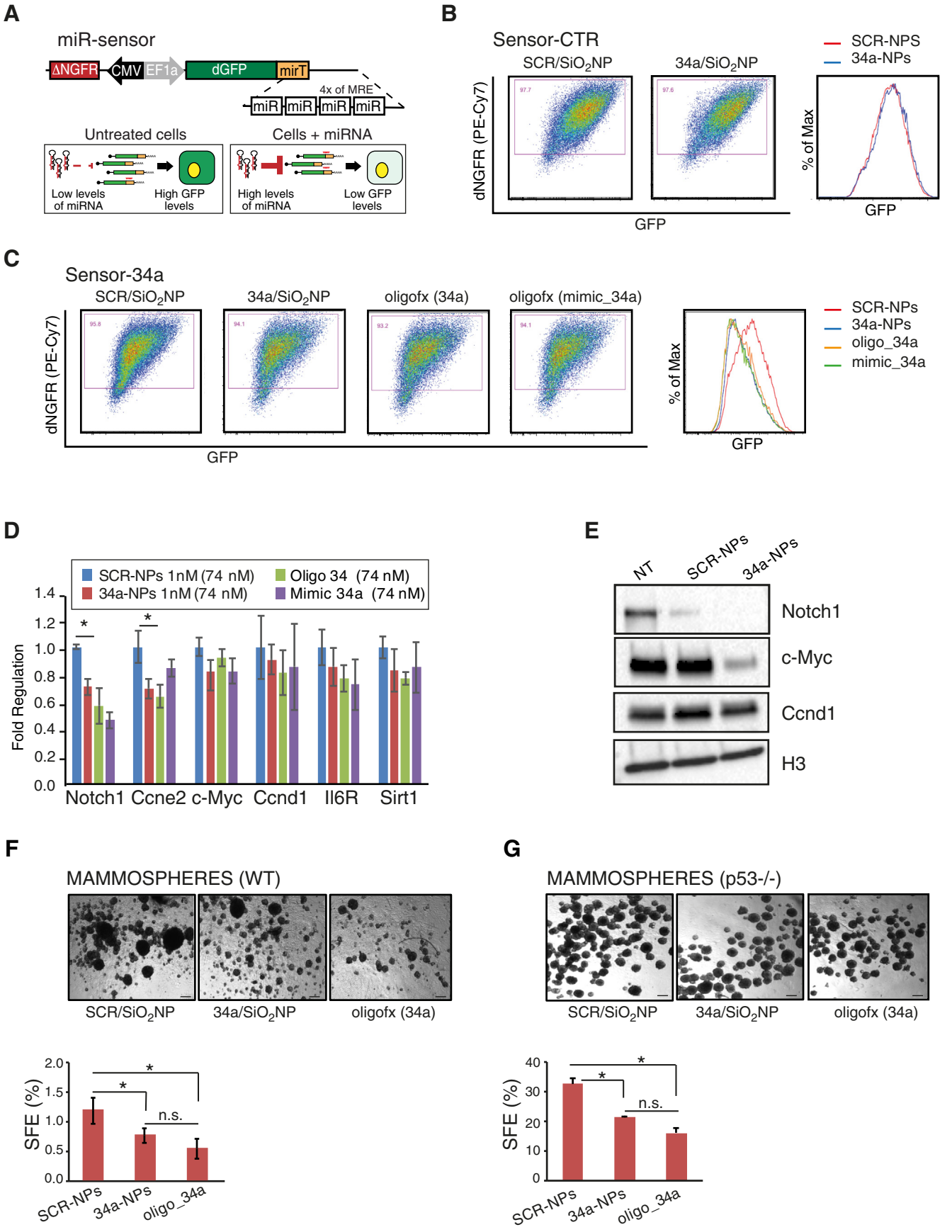
A
miR-sensor
ΔNGFR
CMV
EF1a
dGFP
mirT
4x of MRE
miR
miR
miR
miR
Untreated cells
Cells + miRNA
Low levels of miRNA
High GFP levels
High levels of miRNA
Low GFP levels
B
Sensor-CTR
SCR/SiO2NP
34a/SiO2NP
dNGFR (PE-Cy7)
GFP
SCR-NPS
34a-NPs
% of Max
GFP
C
Sensor-34a
SCR/SiO2NP
34a/SiO2NP
oligofx (34a)
oligofx (mimic_34a)
dNGFR (PE-Cy7)
GFP
% of Max
GFP
SCR-NPs
34a-NPs
oligo_34a
mimic_34a
D
SCR-NPs 1nM (74 nM)
34a-NPs 1nM (74 nM)
Oligo 34 (74 nM)
Mimic 34a (74 nM)
Fold Regulation
Notch1
Ccne2
c-Myc
Ccnd1
Il6R
Sirt1
E
NT
SCR-NPs
34a-NPs
Notch1
c-Myc
Ccnd1
H3
F
MAMMOSPHERES (WT)
SCR/SiO2NP
34a/SiO2NP
oligofx (34a)
SFE (%)
n.s.
SCR-NPs
34a-NPs
oligo_34a
G
MAMMOSPHERES (p53-/-)
SCR/SiO2NP
34a/SiO2NP
oligofx (34a)
SFE (%)
n.s.
SCR-NPs
34a-NPs
oligo_34a

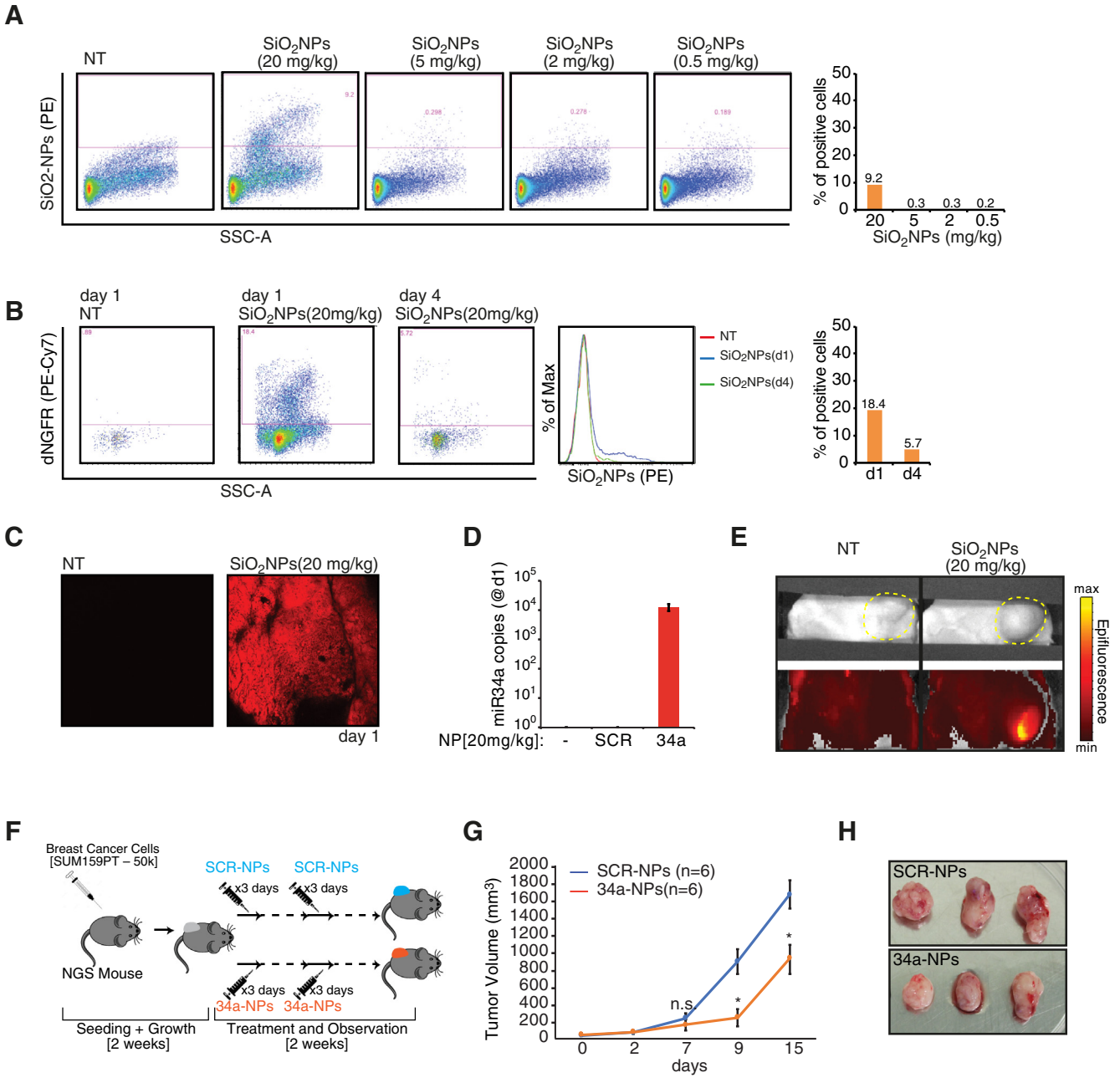

Figure 6. *In vivo* efficacy of miR-34a delivered by SiO_2NPs. (A). Internalization of SiO_2NPs in mammary epithelial cells upon intra-nipple injection. Analysis was performed by FACS at 24 hours post treatment and using different doses of NPs. Bar graphs show the percentage of SiO_2NPs positive cells (B). Time course analysis of internalization of SiO_2NPs at 1 and 4 days after injection. Bar graphs show the percentage of SiO_2NPs positive cells (C). Representative confocal images of a mammary gland at 24 hours post treatment was used to confirm the local distribution of SiO_2NPs. (D). miR-34a levels measured by RT-qPCR in mammary epithelial cells from miR34TKO mice. (E). Representative images of *in vivo* fluorescence as determined by IVIS. Tumor mass is highlighted in yellow. (F) Scheme summarizing the protocol for *in vivo* treatment of breast tumors. (G). Tumor volume during the *in vivo* experiment schematized in panel F. Six mice were analyzed per group. (H). Representative images from the tumors harvested after treatments.

Figure 5. Biological activity of internalized SiO_2NPs carrying miR-34a. (A) Scheme of the miRNA sensor, a lentiviral reporter used to monitor miRNA activity by GFP levels, containing two transgenes i) ΔNGFR, a truncated form of the Nerve Growth Factor Receptor (NGFR) to normalize the transduction efficiency, and ii) a Sensor-GFP, containing four repeats of miR-34a perfect match. A control sensor (Sensor-CTR) was generated using unrelated sequence. (B-C). Box plots show GFP levels in Comma Dβ cells infected with Sensor-CTR (B) or Sensor-34a (C) and treated with NPs. Sensor-34a was also treated by standard transfection using synthetic oligo or a commercial available mimic. Histogram shows the GFP level quantification in the four samples. (D). Expression levels of miR-34a targets (Notch1, Ccne2, c-Myc, Ccnd1, Il6R and Sirt1) measured by RT-qPCR in Comma Dβ upon various treatments. Snord72 served as housekeeping. Asterisks mark significant differences (Student's T-test). (E). Protein levels of miR-34a targets (Notch1, c-Myc and Ccnd1) assessed by western blot in Comma Dβ upon treatment with SiO_2NPs (2 nM). Histone-H3 (H3) served as loading control. (F). Images of mammospheres from wild-type (WT) and p53-null mice after treatment with SiO_2NPs (SCR or 34a) and transfection with mimic-34a. Sphere-forming efficiency (SFE) of three independent experiments (average and st.dev) is shown. Asterisks mark significant differences (Student's *t* test).

SCR-NPs (20 mg/kg) was repeated for 3 consecutive days, 2 weeks in a row (Figure 6, *F*) while tumor masses were continuously analyzed. Importantly, in mice (n = 6) treated with 34a-NPs we observed a significant reduction in tumor growth in comparison to mice treated with SCR-NPs (Figure 6, *G* and *H*). Of note, we could not detect any significant difference between the two groups in the first week of treatment (7 days, Figure 6, *H*). However, substantial effects emerged during the second week (9–15 days, Figure 6, *H*). Tumor masses treated with 34a-NPs were smaller (Figure 5, *G*), further demonstrating that miR-34a delivered *via* SiO_2NPs was able to exert a tumor suppressive function *in vivo*. Overall, these results indicated that SiO_2NPs are a suitable means of intra-tumor local delivery of miR-34a and can be considered for future clinical studies.

Discussion

In this study, we explored the potential of the well-characterized synthetic carrier silica dioxide nanoparticles (SiO_2NPs)[24,29–31] for the delivery of biologically active miRNA mimics. We focused on the tumor-suppressor miR-34a, which is by-and-large one of the most promising therapeutic miRNAs, in particular for the cancers of the breast. We showed that SiO_2NPs efficiently delivered miR-34a as a biological active molecule. With the use of 34a-NPs, we could induce silencing of miR-34a targets either in the form of artificial molecule (miR-sensor) or as endogenous RNAs (e.g. Notch1, Ccne2). Furthermore, using primary mammary cells as recipients, we saw a reduction in mammospheres growth, a phenotype specifically associated with miR-34a activity. The successful outcome of miR-34a delivery was unambiguous, as it was observed using cells that are *per se* devoid of any endogenous miR-34a molecule (miRNA knock-out models) and was accurately quantified using absolute quantification approaches. Efficiency of delivery was evaluated using lipofection as benchmark. This is a relative simple and most efficient methodology for delivering miRNA into cells. However, it can only be applied to cultured cells as it is known to be unsuitable to clinical settings. When compared to lipofection, the amount of miRNA delivered by SiO_2NPs (as total molecules) was in the same range although lower. However, the silencing activity and biological effects were totally comparable. This likely reflects the fact that the RISC complexes on which miRNA molecules are loaded and which mediate miRNA functions, are being saturated thus making the extra amount of miRNA delivered by lipofection not functional. Therefore, miR-34a delivery by SiO_2NPs is actually as effective as by lipofection, with the additional advantage of being applicable to physiologically relevant and clinical settings. Encouraging results were also obtained when using 34a-NPs to reconstitute *in vivo* the expression of miR-34a that had been lost or suppressed through genetic alterations (as in cancer). Indeed, we observed a significant uptake of miR-34a by epithelial cells, which was characterized by fluorescence with a limited spread and, apparently, a quick turnover of molecules. To see the effects of 34a-NPs in an *in vivo* setting, we simulated cancer treatment with a xenograft tumor generated using SUM159pt, which reproduce the most aggressive subtype of breast cancer (the triple-negative claudine-low subtype). These tumors present very limited options for treatment, as they respond poorly to conventional therapies. Nevertheless, the intra-tumor administration of 34a-NPs led to a significant reduction in tutor growth, which was comparable to that previously observed using transgenic models able to activate miR-34a expression in all their cells.[15] Hence, SiO_2NPs can efficiently delivery biologically active miR-34a *in vivo* too. Recently, miRNA based therapeutics have been translated to the bedside showing, on one side, encouraging results in the treatment of different diseases, such as heart failure, atherosclerosis and HCV infection,[23] but, on the other side, unforeseeable adverse effects. The first miRNA to reach phase I in clinical trials looking for cancer treatments was a mimic of miR-34a (*i.e.* Mirna Therapeutics Halts Phase 1 Clinical Study of MRX34) but its testing was abandoned due to unexpected immune-related toxicity. At the moment, it is not known whether the immune system response was elicited by the miRNA itself or by the liposome-formulated method used to deliver it, given that both small RNAs and liposomes are known to induce immune response.[42] Nevertheless, a search for alternative and safe ways to successfully deliver miRNAs in general, and miR-34a in particular, is still underway. Our results clearly show that SiO_2NPs might represent a viable alternative. We are fully aware that, in view of potential clinical applications, relevant issues need to be fully addressed, for instance by testing different ways of administering 34a-NPs (*i.e.* local *vs.* systemic), or by developing a selective way of targeting cancer cells through receptor/ligand binding. In addition, more experiments are needed to clarify what the *in vivo* clearance of 34a-NPs and their (possible) interaction with the immune response are. We believe, nonetheless, to have generated promising results in the right direction and to have made a mark in the development of possible future applications of 34a-NPs in human cancer.

Appendix A. Supplementary data

Supplementary data to this article can be found online at https://doi.org/10.1016/j.nano.2019.03.013.

References

1. Bartel DP. MicroRNAs: genomics, biogenesis, mechanism, and function. *Cell* 2004;**116**:281-97.
2. Bartel DP. MicroRNAs: target recognition and regulatory functions. *Cell* 2009;**136**:215-33.
3. Lujambio A, Lowe SW. The microcosmos of cancer. *Nature* 2012;**482**:347-55.
4. Bader AG, Brown D, Winkler M. The promise of microRNA replacement therapy. *Cancer Res* 2010;**70**:7027-30.
5. Esquela-Kerscher A, Slack FJ. Oncomirs - microRNAs with a role in cancer. *Nat Rev Cancer* 2006;**6**:259-69.
6. Medina PP, Nolde M, Slack FJ. OncomiR addiction in an in vivo model of microRNA-21-induced pre-B-cell lymphoma. *Nature* 2010;**467**:86-90.
7. He L, He X, Lim LP, de Stanchina E, Xuan Z, Liang Y, et al. A microRNA component of the p53 tumour suppressor network. *Nature* 2007;**447**:1130-4.
8. Hermeking H. The miR-34 family in cancer and apoptosis. *Cell Death Differ* 2010;**17**:193-9.
9. Slabakova E, Culig Z, Remsik J, Soucek K. Alternative mechanisms of miR-34a regulation in cancer. *Cell Death Dis* 2017;**8**:e3100.

10. Yang S, Li Y, Gao J, Zhang T, Li S, Luo A, et al. MicroRNA-34 suppresses breast cancer invasion and metastasis by directly targeting Fra-1. *Oncogene* 2013;**32**:4294-303.
11. Bayraktar R, Ivan C, Bayraktar E, Kanlikilicer P, Kabil NN, Kahraman N, et al. Dual Suppressive Effect of miR-34a on the FOXM1/eEF2-Kinase Axis Regulates Triple-Negative Breast Cancer Growth and Invasion. *Clin Cancer Res* 2018;**24**:4225-41.
12. Park EY, Chang E, Lee EJ, Lee HW, Kang HG, Chun KH, et al. Targeting of miR34a-NOTCH1 axis reduced breast cancer stemness and chemoresistance. *Cancer Res* 2014;**74**:7573-82.
13. Kang L, Mao J, Tao Y, Song B, Ma W, Lu Y, et al. MicroRNA-34a suppresses the breast cancer stem cell-like characteristics by downregulating Notch1 pathway. *Cancer Sci* 2015;**106**:700-8.
14. Ma W, Xiao GG, Mao J, Lu Y, Song B, Wang L, et al. Dysregulation of the miR-34a-SIRT1 axis inhibits breast cancer stemness. *Oncotarget* 2015;**6**:10432-44.
15. Bonetti P, Climent M, Panebianco F, Tordonato C, Santoro A, Marzi MJ, et al. Dual role for miR-34a in the control of early progenitor proliferation and commitment in the mammary gland and in breast cancer. *Oncogene* 2019;**38**:360-74.
16. Liu S, Wicha MS. Targeting breast cancer stem cells. *J Clin Oncol* 2010;**28**:4006-12.
17. Chiu YL, Rana TM. siRNA function in RNAi: a chemical modification analysis. *RNA* 2003;**9**:1034-48.
18. Herrera-Carrillo E, Liu YP, Berkhout B. Improving miRNA Delivery by Optimizing miRNA Expression Cassettes in Diverse Virus Vectors. *Hum Gene Ther Methods* 2017;**28**:177-90.
19. van Rooij E, Kauppinen S. Development of microRNA therapeutics is coming of age. *EMBO Mol Med* 2014;**6**:851-64.
20. Farina NH, Zingiryan A, Vrolijk MA, Perrapato SD, Ades S, Stein GS, et al. Nanoparticle-based targeted cancer strategies for non-invasive prostate cancer intervention. *J Cell Physiol* 2018;**233**:6408-17.
21. Yang Y, Yu C. Advances in silica based nanoparticles for targeted cancer therapy. *Nanomedicine* 2016;**12**:317-32.
22. Chaudhary V, Jangra S, Yadav NR. Nanotechnology based approaches for detection and delivery of microRNA in healthcare and crop protection. *J Nanobiotechnology* 2018;**16**:40.
23. Rupaimoole R, Slack FJ. MicroRNA therapeutics: towards a new era for the management of cancer and other diseases. *Nat Rev Drug Discov* 2017;**16**:203-22.
24. Bardi G, Malvindi MA, Gherardini L, Costa M, Pompa PP, Cingolani R, et al. The biocompatibility of amino functionalized CdSe/ZnS quantum-dot-Doped SiO2 nanoparticles with primary neural cells and their gene carrying performance. *Biomaterials* 2010;**31**:6555-66.
25. Guarnieri D, Malvindi MA, Belli V, Pompa PP, Netti P. Effect of silica nanoparticles with variable size and surface functionalization on human endothelial cell viability and angiogenic activity. *J Nanopart Res* 2014;**16**.
26. Low SP, Voelcker NH, Canham LT, Williams KA. The biocompatibility of porous silicon in tissues of the eye. *Biomaterials* 2009;**30**:2873-80.
27. Park JH, Gu L, von Maltzahn G, Ruoslahti E, Bhatia SN, Sailor MJ. Biodegradable luminescent porous silicon nanoparticles for in vivo applications. *Nat Mater* 2009;**8**:331-6.
28. Sabella S, Carney RP, Brunetti V, Malvindi MA, Al-Juffali N, Vecchio G, et al. A general mechanism for intracellular toxicity of metal-containing nanoparticles. *Nanoscale* 2014;**6**:7052-61.
29. Malvindi MA, Brunetti V, Vecchio G, Galeone A, Cingolani R, Pompa PP. SiO2 nanoparticles biocompatibility and their potential for gene delivery and silencing. *Nanoscale* 2012;**4**:486-95.
30. Bitar A, Ahmad NM, Fessi H, Elaissari A. Silica-based nanoparticles for biomedical applications. *Drug Discov Today* 2012;**17**:1147-54.
31. Slowing II, Vivero-Escoto JL, Wu CW, Lin VS. Mesoporous silica nanoparticles as controlled release drug delivery and gene transfection carriers. *Adv Drug Deliv Rev* 2008;**60**:1278-88.
32. Cicalese A, Bonizzi G, Pasi CE, Faretta M, Ronzoni S, Giulini B, et al. The tumor suppressor p53 regulates polarity of self-renewing divisions in mammary stem cells. *Cell* 2009;**138**:1083-95.
33. Deugnier MA, Faraldo MM, Teuliere J, Thiery JP, Medina D, Glukhova MA. Isolation of mouse mammary epithelial progenitor cells with basal characteristics from the Comma-Dbeta cell line. *Dev Biol* 2006;**293**:414-25.
34. Brown BD, Gentner B, Cantore A, Colleoni S, Amendola M, Zingale A, et al. Endogenous microRNA can be broadly exploited to regulate transgene expression according to tissue, lineage and differentiation state. *Nat Biotechnol* 2007;**25**:1457-67.
35. Concepcion CP, Han YC, Mu P, Bonetti C, Yao E, D'Andrea A, et al. Intact p53-dependent responses in miR-34-deficient mice. *PLoS Genet* 2012;**8**e1002797.
36. Corvaglia S, Guarnieri D, Pompa PP. Boosting the therapeutic efficiency of nanovectors: exocytosis engineering. *Nanoscale* 2017;**9**:3757-65.
37. Dontu G, Abdallah WM, Foley JM, Jackson KW, Clarke MF, Kawamura MJ, et al. In vitro propagation and transcriptional profiling of human mammary stem/progenitor cells. *Genes Dev* 2003;**17**:1253-70.
38. Rokavec M, Li H, Jiang L, Hermeking H. The p53/miR-34 axis in development and disease. *J Mol Cell Biol* 2014;**6**:214-30.
39. Bouras T, Pal B, Vaillant F, Harburg G, Asselin-Labat ML, Oakes SR, et al. Notch signaling regulates mammary stem cell function and luminal cell-fate commitment. *Cell Stem Cell* 2008;**3**:429-41.
40. Liu C, Kelnar K, Liu B, Chen X, Calhoun-Davis T, Li H, et al. The microRNA miR-34a inhibits prostate cancer stem cells and metastasis by directly repressing CD44. *Nat Med* 2011;**17**:211-5.
41. Bu P, Chen KY, Chen JH, Wang L, Walters J, Shin YJ, et al. A microRNA miR-34a-regulated bimodal switch targets Notch in colon cancer stem cells. *Cell Stem Cell* 2013;**12**:602-15.
42. De Paula D, Bentley MV, Mahato RI. Hydrophobization and bioconjugation for enhanced siRNA delivery and targeting. *RNA* 2007;**13**:431-56.